

# Nanosecond Dynamics of G $\alpha$ 1 Bound to Nucleotides or Ric-8A, a G $\alpha$ Chaperone with GEF Activity

Labe A. Black,<sup>1,2</sup> Celestine J. Thomas,<sup>1,2</sup> Gwendolyn N. Nix,<sup>1,3</sup> Michelle C. Terwilliger,<sup>1,2</sup> Stephen R. Sprang,<sup>1,3,\*</sup> and J. B. Alexander Ross<sup>1,2,\*</sup>

<sup>1</sup>Center for Biomolecular Structure and Dynamics, <sup>2</sup>Department of Chemistry and Biochemistry, and <sup>3</sup>Division of Biological Sciences, University of Montana, Missoula, Montana

**ABSTRACT** Resistance to Inhibitors of Cholinesterase A (Ric-8A) is a 60-kDa cytosolic protein that has chaperone and guanine nucleotide exchange (GEF) activity toward heterotrimeric G protein  $\alpha$  subunits of the i, q, and 12/13 classes, catalyzing the release of GDP from G $\alpha$  and subsequent binding of GTP. In the absence of GTP or GTP analogs, and subsequent to GDP release, G $\alpha$  forms a stable nucleotide-free complex with Ric-8A. In this study, time-resolved fluorescence anisotropy measurements were employed to detect local motions of G $\alpha$ 1 labeled at selected sites with Alexa 488 (C5) fluorescent dye (Ax) in the GDP, GTP $\gamma$ S (collectively, GXP), and Ric-8A-bound states. Sites selected for Alexa 488 (C5) derivatization were in the  $\alpha$ -helical domain (residue 106), the  $\alpha$ -helical domain-Ras-like domain hinge (residue 63), Switch I (residue 180), Switch II (residue 209), Switch III (residue 238), the  $\alpha$ 4 helix (residue 305), and at the junction between the purine-binding subsite in the  $\beta$ 6- $\alpha$ 5 loop and the C-terminal  $\alpha$  helix (residue 330). In the GXP-bound states, the Alexa fluorophore reports local motions with correlation times ranging from 1.0 to 1.8 ns. The dynamics at Ax180 is slower in G $\alpha$ 1•GDP than in G $\alpha$ 1•GTP $\gamma$ S. The reverse is true at Ax209. The order parameters,  $S^2$ , for Alexa probes at switch residues are high (0.78–0.88) in G $\alpha$ 1•GDP and lower (0.67–0.75) in G $\alpha$ 1•GTP $\gamma$ S, although in crystal structures, switch segments are more ordered in the latter. Local motions at Ax63, Ax180, Ax209, and Ax330 are all markedly slower (2.3–2.8 ns) in G $\alpha$ 1:Ric-8A than in G $\alpha$ 1•GXP, and only modest ( $\pm 0.1$ ) differences in  $S^2$  are observed at most sites in G $\alpha$ 1:Ric-8A relative to G $\alpha$ 1•GXP. The slow dynamics suggests long-range correlated transitions within an ensemble of states and, particularly in the hinge and switch segments that make direct contact with Ric-8A. Induction of G $\alpha$ 1 structural heterogeneity by Ric-8A provides a mechanism for nucleotide release.

## INTRODUCTION

Heterotrimeric G proteins relay signals elicited by the binding of agonists to seven-transmembrane G protein-coupled receptors (GPCRs), a process that occurs predominantly at the plasma membrane (1). Engagement of G protein heterotrimers composed of a GDP-bound alpha subunit (G $\alpha$ ) and a heterodimer of beta and gamma subunits (G $\beta\gamma$ ) by GPCRs induces the release of GDP from G $\alpha$ . Subsequent binding of GTP by G $\alpha$  and its full or partial release from heterodimeric G $\beta\gamma$  yield an activated G $\alpha$ •GTP species that is free to bind

and regulate cellular effectors. Upon hydrolysis of GTP, by virtue of its intrinsic or GTPase-activating, protein-stimulated GTPase activity, G $\alpha$  reassociates with G $\beta\gamma$ , thereby terminating effector regulation (2). Proteins that catalyze exchange of GDP for GTP, such as GPCRs, are known as guanine-exchange factors (GEFs). Cytoplasmic proteins with GEF activity have been identified. Notable among these are the A and B isoforms of Ric-8, which have been shown to act as GEFs for free G $\alpha$ •GDP subunits that are not associated with G $\beta\gamma$ . Ric-8A is a soluble, cytosolic 60-kDa protein that exhibits specificity for the i, q, and 12/13 classes of G $\alpha$  subunits and accelerates the rate of nucleotide exchange in vitro (3), whereas Ric-8B interacts specifically with G $\alpha$ s and G $\alpha$ olf (4). Ric-8 homologs have been associated with several cell-biological processes (5,6) and also have been shown to serve as G $\alpha$  chaperones in cells, which are required for the biogenesis of functional G $\alpha$  subunits and their localization in cellular membrane

Submitted February 18, 2016, and accepted for publication July 11, 2016.

\*Correspondence: [sandy.ross@umontana.edu](mailto:sandy.ross@umontana.edu) or [stephen.sprang@umontana.edu](mailto:stephen.sprang@umontana.edu)

Labe A. Black's present address is Rensselaer Polytechnic Institute, Troy, New York.

Celestine J. Thomas's present address is Regeneron Pharmaceuticals, Inc., Tarrytown, New York.

Editor: Elizabeth Rhoades.

<http://dx.doi.org/10.1016/j.bpj.2016.07.021>

© 2016 Biophysical Society.

compartments (7). Whether Ric-8A GEF activity has a direct role in regulation of cell signaling processes remains under investigation (8).

G $\alpha$  subunits are members of the Ras superfamily of GTPases. The Ras-like domain (RD) of G $\alpha$  (Fig. 1) includes two elements (Switch I and Switch II) that comprise residues involved in catalysis, Mg<sup>2+</sup> cofactor binding, and, in the case of Switch II, effector binding. Both undergo conformational changes and order  $\rightarrow$  disorder transitions upon GTP hydrolysis (9–11). Unique to G $\alpha$  is a  $\sim$ 120-residue  $\alpha$ -helical domain (HD) that is inserted at the N-terminus of Switch I. Although it forms interactions only with the ribosyl moiety of GDP and GTP (12,13), the HD acts as a lid, restricting egress of the guanine nucleotide from its binding pocket. Much has been learned about GEF-stimulated nucleotide exchange in heterotrimeric G-proteins from the perspective of GPCR-mediated G protein activation (14). Recent spectroscopic and crystallographic studies have demonstrated that GPCRs induce major domain rearrangements as well as perturbations of local structural elements in G $\alpha$  subunits (15,16). The RD and HD separate upon formation of an agonist-activated GPCR:G protein complex (15–17). Recent microsecond-scale molecular-dynamics calculations indicate that domain separation is necessary but not sufficient for nucleotide release from G $\alpha$ , as other rearrangements at the RD-HD interface are also necessary to destabilize bound nucleotide (18).

Ric-8A induces structural changes in G $\alpha$  subunits that are consistent with its GEF and chaperone activity. Together, experiments employing heteronuclear NMR, global hydrogen-deuterium exchange, limited proteolysis, and scanning calorimetry indicate that Ric-8A stabilizes a structurally heterogeneous and conformationally dynamic state of nucleotide-free G $\alpha$ 1 (19). Double electron-electron resonance experiments demonstrate that upon binding to Ric-8A and release of GDP, the RD and HD swing apart and assume multiple conformational states (20). The RD itself exhibits structural plasticity in this complex, as reported by the distribution of distances between spin-label probes at the nucleotide-binding site, switch segments, and the RD-HD hinge. Thus, in stabilizing the nucleotide-free state, Ric-8A induces or permits major structural perturbations of G $\alpha$  tertiary and possibly secondary structure.

In this investigation, we aimed to explore differences in local structural dynamics associated with nucleotide-bound and Ric-8A-stabilized nucleotide-free states of G $\alpha$ 1. By measuring time-resolved fluorescence anisotropy of Alexa dyes conjugated at selected sites on the solvent-accessible surface of G $\alpha$ 1, we resolved the timescales and amplitudes of local structural motions that correlate with equilibrium conformational dynamics in G $\alpha$ 1•GDP, G $\alpha$ 1•GTP $\gamma$ S, and G $\alpha$ 1:Ric-8A. We found that the correlation times of the local motions were typically longer at most sites in the Ric-8A-bound complex of G $\alpha$ 1. In contrast, differences in the amplitude of local dynamics observed in the three G $\alpha$ 1 complexes were highly site specific. The data reveal surprising differences between GDP-bound and GTP-bound states that are not evident from crystal structures, and demonstrate that the global perturbations of G $\alpha$  structure in the nucleotide-empty, Ric-8A-bound state are complemented by comparable changes in local secondary-structure dynamics.

## MATERIALS AND METHODS

### Protein expression and purification

A cDNA construct encoding rat Hexa I G $\alpha$ 1 (21), which harbors six amino acid substitutions at solvent-exposed cysteine residues (C3S-C66A-C214S-C305S-C325A-C351I) and a hexa-histidine tag between amino acid residues M119 and T120, was subcloned into a pDEST-15 destination vector for expression as a GST fusion protein (20). This vector was used as a template for construction of single cysteine-substitution mutants (E63C, Q106C, K180C, K209C, E238C, S305C (which restored the cysteine in the native sequence), and K330C, respectively). Hexa I G $\alpha$ 1 cysteine-substitution mutants were expressed and purified as described previously (19). A fragment of rat Ric-8A composed of residues 1–491, which was found to have GEF activity exceeding that of the full-length protein, was expressed and purified as described previously (19) and used for all experiments.

### Protein fluorescent-dye labeling

The Hexa I G $\alpha$ 1 cysteine-substitution mutants (E63C, Q106C, K180C, K209C, E238C, C/S305C, and K330C; 100–200  $\mu$ M) were incubated in reducing buffer (50 mM Tris pH 8.0, 250 mM NaCl, 100  $\mu$ M GDP, 10 mM dithiothreitol) for 30 min and subsequently exchanged into labeling buffer (20 mM MOPS pH 7.4, 250 mM NaCl, 100  $\mu$ M GDP, 10% glycerol) using Millipore Amicon Ultra concentrators (30 kDa cutoff; Merck Millipore, Billerica, MA). Then, 100–200  $\mu$ L of 100- $\mu$ M reduced protein

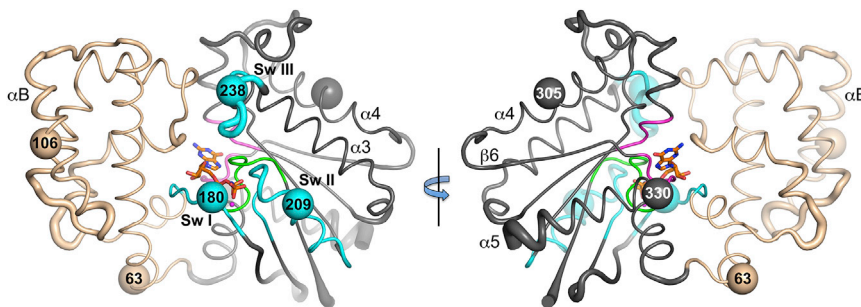


FIGURE 1 Ribbon schematic of the tertiary structure of G $\alpha$ 1•GppNHp (PDB: 1CIP). The  $\alpha$ -helical and Ras-like domains are colored beige and charcoal, respectively. Switch segments (Sw I–III) are colored cyan and labeled. The P-loop and purine-binding segments are colored cyan and magenta, respectively. Secondary-structure elements of interest (see text) are labeled. Alexa 488 (C5)-conjugated residues are shown as spheres and labeled.

sample was allowed to react with equimolar Alexa 488 (C5) maleimide (100–200 nmol stock aliquots; ThermoFisher Scientific, Waltham, MA). Reactions were quenched after 15 min by addition of  $\beta$ -mercaptoethanol to a final concentration of 10 mM, passed over a 10-mL G-10 desalting column (GE Healthcare Life Sciences, Marlborough, MA) to remove unreacted dye, and then passed through a 0.22- $\mu$ m filter to remove aggregated protein. Labeled proteins were subjected to mass spectrometry analysis using a Microflex matrix-assisted laser desorption/ionization time-of-flight (MALDI-TOF) instrument (Bruker, Billerica, MA).

## Preparation of G $\alpha$ i1 complexes and nucleotide-exchange assays

Freshly labeled G $\alpha$ i1 samples were diluted to 1  $\mu$ M in 20 mM Hepes pH 8.0, 100 mM NaCl, 2 mM dithiothreitol, 0.01% C12E10 with either 100  $\mu$ M GDP to stabilize the G $\alpha$ i1•GDP complex, 1.5  $\mu$ M Ric-8A to form the nucleotide-free G $\alpha$ i1:Ric-8A complex, or 1.5  $\mu$ M Ric-8A + 10  $\mu$ M GTP $\gamma$ S + 10 mM Mg<sup>2+</sup> to employ the GEF activity of Ric-8A to catalyze formation of G $\alpha$ i1•GTP $\gamma$ S. After a 30-min incubation on ice, to separate nucleotide-bound G $\alpha$ i1 from the Ric-8A-bound species, the samples were purified by gel filtration on a Superdex S-200 (GE) size-exclusion column at a flow rate of 0.4 mL/min using an ÄKTA fast protein liquid chromatography system (GE) and monitored at 280 nm. Column fractions corresponding to 40 kDa (15.2-mL elution volume, G $\alpha$ i1•GDP or G $\alpha$ i1GTP $\gamma$ S) or 95 kDa (12.5-mL elution volume, G $\alpha$ i1:Ric-8A) were pooled and an additional binding partner (either 100  $\mu$ M GDP, 1  $\mu$ M Ric-8A, or 10  $\mu$ M GTP $\gamma$ S with 10 mM Mg<sup>2+</sup>) was added. These partner concentrations ensured saturation binding and were used for data acquisition. Rates of Ric-8A-catalyzed GTP $\gamma$ S binding to G $\alpha$ i1 were determined using an intrinsic tryptophan fluorescence assay as described previously (19).

## Fluorescence lifetime and time-resolved anisotropy decay

For intensity and anisotropy decay measurements, we employed time-correlated single-photon counting using the FLASC 1000 sample chamber (Quantum Northwest, Liberty Lake, WA) as described previously (22). We analyzed the intensity and anisotropy decay data using the software package FluoFit Pro v4.6.6.0 (PicoQuant, Berlin, Germany). Representative data are provided in Figs. S4–S6 in the Supporting Material.

## Fluorescence correlation spectroscopy

Translational diffusion coefficients were obtained from fluorescence correlation spectroscopy (FCS) measurements carried out with an inverted-confocal Olympus FluoView IX71 microscope fitted with a 60 $\times$  1.2-NA water objective (Olympus, Center Valley, PA). A 468-nm pulsed-diode laser (20–60  $\mu$ W at 20 MHz; model LDH-P-C-485; PicoQuant) was used for excitation. The emission was selected using a 535/50-nm bandpass filter (Chroma, Bellows Falls, VT), and avalanche photodiodes (optoelectronic photon-counting module model SPCM-AQR-14-FC; Perkin-Elmer, Waltham, MA) were used for detection. A  $\beta$ -ME adduct of Alexa 488 (C5) was used to optimize the confocal optical train, and the confocal volume properties were determined using a translational diffusion coefficient of  $420 \pm 5 \mu\text{m}^2 \text{s}^{-1}$  at 21.5°C (value and range calculated from literature values) (23–25). SymPhoTime v5.3.2.2 (PicoQuant) was used for both data acquisition and analysis.

## Theoretical considerations and analysis model

The fluorescence anisotropy decay kinetics of an immobile probe attached to a rigid ellipsoid can be described by a sum of five exponential terms (26).

However, three correlation times at most might be resolved for ellipsoids of varying ratios, because two pairs of correlation times are essentially degenerate (27). As discussed by Lakowicz (28), however, the overall hydrodynamic behavior of many soluble, globular proteins may be adequately described by a single rotational correlation time. If there were also local motion in a region of the protein containing the probe, there would be additional depolarization of the fluorescence, and fitting the anisotropy decay,  $r(t)$ , as a sum of exponentials would yield two correlation times,  $\phi_{\text{short}}$  and  $\phi_{\text{long}}$ . Accordingly,

$$r(t) = r_0 \left[ p e^{\frac{-t}{\phi_{\text{short}}}} + (1-p) e^{\frac{-t}{\phi_{\text{long}}}} \right], \quad (1)$$

where  $p$  is a weighting factor between 0 and 1, and  $r_0$  is the frozen, or limiting, anisotropy at time zero;  $r_0(1-p) = \beta_{\text{long}}$  and  $r_0 p = \beta_{\text{short}}$ . The longer rotational correlation time reflects the overall rotation motion of the protein (referred to as the global rotation), whereas the shorter rotational correlation time contains contributions from both local and global motions:

$$\phi_{\text{short}}^{-1} = \phi_{\text{local}}^{-1} + \phi_{\text{global}}^{-1}; \quad \phi_{\text{long}}^{-1} = \phi_{\text{global}}^{-1}. \quad (2)$$

NMR (29) and molecular-dynamics studies (30) suggest that collective librational motions of the cysteine side chain and within the Alexa 488 (C5) side chain could produce an anisotropy decay component with a correlation time on the order of  $\leq 100$  ps. These motions would not be resolved by our experiments, which would result in smaller  $r_0$  values than would be expected for Alexa 488 (31). Other local motions, such as reorientation of the Alexa fluorophore, are expected to have correlation times in the nanosecond range (32,33), which is the time range of the intensity decay of Alexa 488 (C5) ( $\sim 4$  ns). The global motion of the Ric-8A complex, however, is an order of magnitude slower, and thus is too slow for accurate resolution by Alexa 488 (C5). Therefore, we calculated the correlation time for global rotational motion ( $\phi_{\text{global}}$ ) from the average translational diffusion coefficient of the G $\alpha$ i1-Alexa adducts and their complexes with Ric-8A, respectively, by using the Stokes-Einstein-Debye relations (28,34). FCS was used to determine the translational diffusion coefficients (Table 1; Fig. S6, A and B). In the analysis of anisotropy decay data, the calculated  $\phi_{\text{global}}$  values derived from FCS were used as fixed parameters. The local correlation times and fractions  $\beta_{\text{short}}$  recovered from this fitting procedure are relative to each other and provide a direct comparison of the local structural dynamics, on the low nanosecond timescale, that occurs within G $\alpha$ i1 in the various binding states.

To model G $\alpha$ i1 local motions, we employed both the wobble-in-a-cone model (square-well potential) and the order parameter  $S^2$  (28,35). The wobble-in-a-cone model assumes that the anisotropy component with

**TABLE 1** Translational Diffusion Coefficients of G $\alpha$ i1 HEXA I Bound to Nucleotide (GDP, GTP $\gamma$ S) or GEF (Ric-8A)

Residue	$D_{\text{translation}} (\mu\text{m}^2 \text{s}^{-1})$		
	GDP	Ric-8A	GTP $\gamma$ S
63	92 (–6, 7)	72 (–7, 8)	95 (–4, 5)
106	93 (–4, 4)	56 (–5, 7)	85 (–6, 7)
180	92 (–6, 7)	69 (–4, 5)	97 (–7, 8)
209	100 (–16, 19)	58 (–6, 7)	86 (–7, 8)
238	108 (–7, 8)	77 (–7, 8)	93 (–4, 5)
305	105 (–9, 10)	50 (–4, 5)	93 (–10, 12)
330	93 (–5, 6)	71 (–3, 3)	99 (–5, 6)
Average	97 (–7, 9)	65 (–5, 6)	92 (–6, 7)

Diffusion coefficients were measured at 21.5°C. Values in parentheses represent uncertainty at the 95% confidence limits as determined by the support-plane method (56).

amplitude  $\beta_{\text{short}}$  reflects motions of the probe within a cone-shaped volume defined by an angle  $\theta$  with respect to the symmetry axis of the cone. The order parameter  $S^2$  ranges from 0 for unrestricted motion ( $\theta = 90^\circ$ ) to 1.0 at complete immobilization ( $\theta = 0^\circ$ ). Smaller cone angles imply greater local restriction and, conversely, larger cone angles imply greater range of motion. The order parameter and cone angles are obtained using the relationship

$$S^2 = \frac{\beta_{\text{long}}}{r_0} = [0.5 \cos \theta (1 + \cos \theta)]^2, \quad (3)$$

where  $r_0$  is the sum of  $\beta_{\text{short}} + \beta_{\text{long}}$ , the amplitudes of the short and long correlation times, respectively. Table 2 reports the order parameters and cone angles for the various Gai1-Alexa 488 (C5) dye conjugates in each binding state.

## RESULTS

Time-resolved fluorescence anisotropy measurements were employed to detect perturbations of the Gai1 secondary-structure dynamics due to binding of Ric-8A, relative to the dynamics of the GDP and GTP $\gamma$ S-bound states. To this end, Alexa 488 (C5) maleimide dyes were installed at cysteine residues introduced by site-directed mutagenesis at solvent-accessible sites within seven functionally important regions of the protein. The cysteine mutations were introduced into a surface-cysteine-free Gai1 construct,

Hexa I (21). The seven cysteine substitutions, each introduced individually, were E63C, located within the N-terminal of the two segments that link the HD of Gai1 to the RD; Q106C, in the  $\alpha$ B helix of the HD; K180C in Switch I; K209C in Switch II; E238C in Switch III; S305C, located in the  $\alpha$ 4 helix of the RD; and K330C, located at the junction of the  $\beta$ 6- $\alpha$ 5 purine-binding loop and the  $\alpha$ 5 helix of the RD (Fig. 1).

After conjugation with Alexa 488 (C5), mass spectrometry analysis indicated derivatization only at the introduced cysteine thiols (Fig. S1). GDP-bound Gai1 Alexa adducts were incubated with Ric-8A in the presence or absence of the nonhydrolyzable GTP analog GTP $\gamma$ S, and subjected to size-exclusion chromatography. The latter condition affords a homogeneous nucleotide-free Gai1:Ric-8A complex. In the presence of GTP $\gamma$ S, Gai1:Ric-8A rapidly dissociated, yielding homogeneous Ric-8A and Gai1•GTP $\gamma$ S, which were well resolved by gel filtration with a Superdex S-200 column. Each of the Alexa-conjugated Gai1 variants (which we refer to by the residue number of the derivatized site preceded by Ax) formed homogeneous complexes with Ric-8A, which in the presence of GTP $\gamma$ S were resolved as free Ric-8A and Gai1•GTP $\gamma$ S. GTP $\gamma$ S binding assays, which followed the increase of intrinsic tryptophan fluorescence upon addition of GTP $\gamma$ S, demonstrated that all of the

**TABLE 2** Time-Resolved Anisotropy Parameters Describing the Dynamics of Alexa 488 (C5) Fluorophores Installed at the Indicated Residues of Gai1 Bound to Nucleotides or Ric-8A

Residue	$S^2 = \beta_{\text{long}}/\Sigma\beta_i$	$\theta^\circ$	$\phi_{\text{local}}$ (ns)	$r_0 = \Sigma\beta_i$	$\chi^2$
<b>Gai1•GDP</b>					
63	0.56 (−0.05, 0.05)	35 (−2, 2)	1.2 (−0.2, 0.3)	0.25 (−0.02, 0.02)	1.17
106	0.47 (−0.03, 0.03)	39 (−2, 2)	1.7 (−0.3, 0.3)	0.26 (−0.02, 0.02)	1.14
180	0.88 (−0.22, 0.27)	16 (−2, 3)	1.3 (−0.5, 0.9)	0.26 (−0.06, 0.08)	1.03
209	0.84 (−0.16, 0.17)	19 (−2, 2)	1.6 (−0.5, 0.8)	0.28 (−0.05, 0.06)	1.11
238	0.78 (−0.12, 0.14)	23 (−2, 2)	1.3 (−0.2, 0.5)	0.29 (−0.04, 0.05)	1.07
305	0.57 (−0.05, 0.06)	34 (−2, 2)	1.0 (−0.2, 0.2)	0.28 (−0.03, 0.03)	1.16
330	0.48 (−0.04, 0.04)	39 (−2, 3)	1.1 (−0.2, 0.2)	0.24 (−0.02, 0.02)	1.13
<b>Gai1:Ric-8A</b>					
63	0.73 (−0.06, 0.06)	26 (−1, 1)	2.3 (−0.5, 0.7)	0.32 (−0.03, 0.03)	1.20
106	0.43 (−0.02, 0.02)	41 (−1, 2)	2.2 (−0.4, 0.4)	0.28 (−0.02, 0.02)	1.17
180	0.77 (−0.07, 0.06)	24 (−2, 1)	2.7 (−0.7, 0.9)	0.32 (−0.03, 0.02)	1.13
209	0.67 (−0.05, 0.05)	29 (−1, 1)	2.8 (−0.6, 0.6)	0.32 (−0.02, 0.02)	1.22
238	0.56 (−0.04, 0.04)	35 (−2, 1)	1.5 (−0.3, 0.3)	0.28 (−0.02, 0.02)	1.15
305	0.47 (−0.03, 0.03)	40 (−2, 1)	1.5 (−0.3, 0.3)	0.27 (−0.02, 0.02)	1.21
330	0.73 (−0.06, 0.06)	26 (−1, 1)	2.3 (−0.5, 0.6)	0.30 (−0.02, 0.02)	1.07
<b>Gai1•GTP<math>\gamma</math>S</b>					
63	0.55 (−0.05, 0.05)	35 (−2, 2)	1.3 (−0.3, 0.3)	0.25 (−0.02, 0.03)	1.15
106	0.48 (−0.03, 0.03)	39 (−2, 2)	1.7 (−0.3, 0.3)	0.27 (−0.02, 0.02)	1.08
180	0.70 (−0.07, 0.07)	28 (−2, 1)	1.8 (−0.4, 0.5)	0.28 (−0.03, 0.03)	1.10
209	0.67 (−0.08, 0.09)	29 (−2, 2)	1.0 (−0.2, 0.2)	0.29 (−0.03, 0.04)	1.30
238	0.75 (−0.10, 0.11)	25 (−2, 2)	1.2 (−0.3, 0.3)	0.33 (−0.04, 0.04)	1.13
305	0.28 (−0.02, 0.03)	50 (−3, 4)	1.2 (−0.2, 0.2)	0.22 (−0.02, 0.02)	1.19
330	0.47 (−0.04, 0.04)	39 (−2, 3)	1.2 (−0.2, 0.2)	0.23 (−0.02, 0.02)	1.14

The local correlation time,  $\phi_{\text{local}}$ , and  $\beta_i$  values were used to model the secondary-structure dynamics for Gai1 in its various binding states (GDP, Ric-8A, and GTP $\gamma$ S-bound) at 25°C. The  $\phi_{\text{local}}$  values were extracted from the short correlation time (Eq. 2), with average  $\phi_{\text{global}}$  values of 15 (−1, 2) ns for the nucleotide complexes and 53 (−4, 4) ns for the Ric-8A complexes, calculated from FCS data (Table 1). The  $\phi_{\text{global}}$  values, calculated from the FCS-determined diffusion coefficients corrected to 25°C, were fixed parameters in the analyses of the anisotropy decay data. The time-zero anisotropy ( $r_0$ ) values were calculated from  $\Sigma\beta_i$  values. The  $\chi^2$  statistic reports on the goodness of the fits for a double exponential decay law. The individual parameter errors were determined at 95% confidence limits using the support-plane method (56), and the propagated uncertainties are reported within parentheses.

Alexa-conjugated *Gai1* variants exhibited intrinsic and Ric-8A-catalyzed GTP $\gamma$ S binding kinetics comparable to that observed for Hexa-I *Gai1* (Fig. S2).

### FCS and fluorescence anisotropy

Example anisotropy decay data and analyses are reported in Figs. S3 and S4. FCS was used to obtain accurate values for the translational diffusion coefficients of dye-conjugated *Gai1* variants and their Ric-8A complexes (Table 1; Fig. S6, A and B).

The *Gai1*•GDP and *Gai1*•GTP $\gamma$ S variants had similar translational diffusion coefficients of 97 (−7, 9)  $\mu\text{m}^2 \text{s}^{-1}$  and 92 (−6, 7)  $\mu\text{m}^2 \text{s}^{-1}$ , respectively, and the *Gai1*:Ric-8A complex had a slower diffusion coefficient of 65 (−5, 6)  $\mu\text{m}^2 \text{s}^{-1}$  (95% confidence limits shown in parentheses). Using the Stokes-Einstein-Debye relations (28,34), these values (Table 1) translate to global-rotational correlation times of 15 (−1, 2) ns and 53 (−4, 4) ns for nucleotide- and Ric-8A-bound states, respectively, at 25°C. The  $\phi_{\text{global}}$  values, calculated from FCS data, were used as fixed parameters in the anisotropy decay analysis. Fixing this parameter reduces cross correlation in the values recovered for the amplitudes ( $\beta_i$ ) associated with local and global rotation and the short rotational correlation time ( $\phi_{\text{short}}$ ). The  $\beta_{\text{long}}$  values reflect the contribution of global motion to the overall fluorescence anisotropy for each *Gai1* conjugate in nucleotide- or Ric-8A-bound states, and were used to calculate the values for the order parameter  $S^2$  and cone angle  $\theta$ . The values for  $\phi_{\text{local}}$  (Table 2) were computed from  $\phi_{\text{short}}$  and  $\phi_{\text{global}}$  by using Eq. 2.

### DISCUSSION

Two parameters that quantify the extent and rate of depolarization, respectively, are the preexponential term ( $\beta_i$ ), from which the order parameter  $S^2$  is derived, and the rotational correlation time ( $\phi_i$ ). In the absence of a complete spatial description of probe dynamics, the barriers that affect depolarization can be described either by the wobble-in-a-cone model or by the order parameter  $S^2$ , as described above (28,35,36). The different magnitudes of the short correlation times, however, do suggest the kinds of motions that might contribute to the depolarization rate. Subnanosecond correlation times are dominated by amino acid side-chain dynamics; shorter local correlation times of a few nanoseconds may be associated, for example, with loop dynamics; and longer local correlation times may be attributed to increased involvement of additional elements of secondary structure, such as whole domain motions (37–40). The results of the cone-angle and order-parameter analyses and a comparison of the timescales of the local motions show how nucleotide binding and the action of the GEF/chaperone Ric-8A influence the dynamic structure of *Gai1*. In the following discussion, we refer to values of  $\phi_{\text{local}}$  (cited with confidence limits)

that differ significantly among the conjugated Alexa 488 (C5) probes, and the order parameter  $S^2$ , which is derived from preexponential values for which confidence limits are fairly uniform across Alexa-derivatization sites and *Gai1*-binding states. These quantities are presented in Table 2 and in graphical form in Figs. 2 and 3, respectively. The heat maps shown in Figs. 4 and 5 illustrate changes in dynamics and local order, respectively, in the progression of *Gai1* from GDP-bound to GTP $\gamma$ S-bound states via the Ric-8A-stabilized nucleotide-free state.

### Alexa dyes probe functionally important *Gai1* sites

We installed Alexa fluorophores at positions that harbor polar or charged side chains in native *Gai1*, and are observed to project into solvent in crystal structures of *Gai1*. We used the Alexa fluorophores to probe local *Gai1* dynamics at the three Switch regions (Ax180 in Switch I, Ax209 in Switch II, and Ax238 in Switch III) that undergo conformational changes upon hydrolysis of GTP to GDP, converting *Gai1* from the canonically active to inactive states for most signaling events (11). These elements form main-chain or side-chain interactions with the  $\gamma$  phosphate of GTP $\gamma$ S and the  $\text{Mg}^{2+}$  cofactor, and thus are sensors of the GTP-bound state (12). Switch III, a mobile polypeptide loop, is N-terminal to the canonical effector-binding site in the  $\alpha 3$  helix and contributes residues to the interface between the RD and HD. All three regions are potential Ric-8A interaction sites. To assess dynamic changes that occur upon nucleotide unbinding and release from *Gai1* as catalyzed by Ric-8A, we probed a residue near the purine-binding site at position 330 and at the hinge between RD and HD at position 63. Residue 330 is located at the junction between the  $\beta 6$ - $\alpha 5$  loop, which contributes part of the purine-binding site, and the  $\alpha 5$  helix, which interacts with both GPCRs and Ric-8A (16,19,41,42). As such, an Alexa probe at this position could potentially report on the communication between the guanine nucleotide- and GEF-binding sites. Domain separation

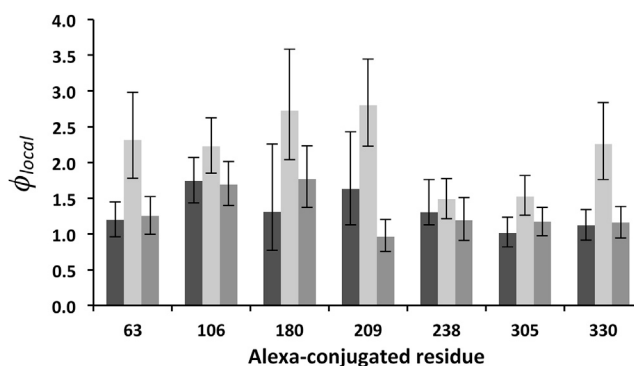


FIGURE 2 Local correlation times reported in Table 2 for each binding state: GDP (dark gray), Ric-8A (light gray), and GTP $\gamma$ S (medium gray). The error bars indicate error propagation of the uncertainty in the fitted correlation times calculated at the 95% confidence limits (56).

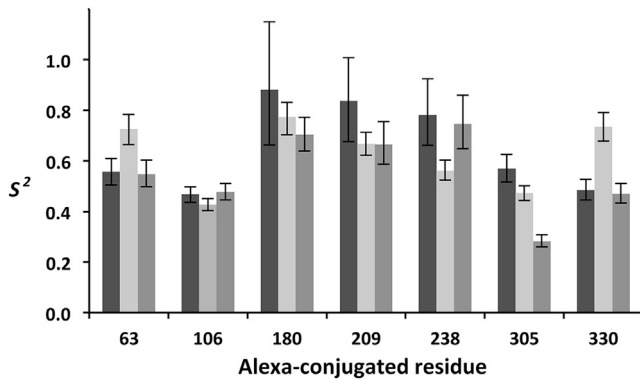


FIGURE 3 Order parameter,  $S^2$ , values reported in Table 2 for each binding state: GDP (dark gray), Ric-8A (light gray), and GTP $\gamma$ S (medium gray). The error bars indicate error propagation of the uncertainty in anisotropy parameters  $\beta_i$  calculated at the 95% confidence limits (56).

induced by Ric-8A binding could potentially perturb local dynamics near the interdomain hinge at position 63. Two residues that are not expected to undergo nucleotide-dependent changes have been labeled: 106 in the HD and 305 in the  $\alpha$ 4 helix. Neither has been shown to exhibit structural changes upon nucleotide binding or hydrolysis, and nitroxide spin labels at these sites are not perturbed upon Ric-8A binding. We do not expect nucleotide- or Ric-8A-dependent changes in dynamics to occur at these sites.

### Local dynamics of nucleotide-bound Gai1

The local correlation times of Alexa-conjugated residues in Gai1•GDP and Gai1•GTP $\gamma$  range between 1 and 1.7 ns

(Table 2). In most cases, the difference in  $\phi_{\text{local}}$  among the sites does not exceed the confidence limits. Alexa probes in the three switch segments report the longest local correlation times. Residues 180 and 209 in Switch I and II, respectively, respond the most markedly to GDP  $\rightarrow$  GTP $\gamma$ S exchange: Ax209 transitions to faster motion ( $\phi_{\text{local}}$ , 1.6  $\rightarrow$  1.0 ns) and Ax180 transitions to slower motion ( $\phi_{\text{local}}$ , 1.3  $\rightarrow$  1.8 ns). The uncertainty in these correlation times is high for Alexa fluorophores at both sites, particularly in the GDP-bound state. Because instrumental and experimental sources of variation are comparable across experiments, the relatively high uncertainty might be explained by the presence of an ensemble of slowly exchanging states, each with a unique correlation time that, if it were sufficiently different, would appear as a broader than usual time distribution (i.e., error function) in a global-local anisotropy decay analysis. This is supported by crystal structures of Gai1•GDP, which show Switch I to be partially disordered and Switch II to be fully disordered, consistent with conformational heterogeneity (43–45). The electron spin resonance (EPR) spectrum for a nitroxide spin label at position 209 is indicative of interconversion between a state exhibiting fast anisotropic motion (possibly the dominant mode reported by fluorescence anisotropy) and one undergoing slower isotropic dynamics in the GDP-bound state (46). Recent relaxation-dispersion experiments demonstrated that residues in all three switch segments in GDP-bound and nucleotide-free Gai1 show dynamics in the microsecond-to-millisecond timescale (47). Taken together, the data show that nucleotide-sensitive structural elements in Gai1 undergo a range of dynamic

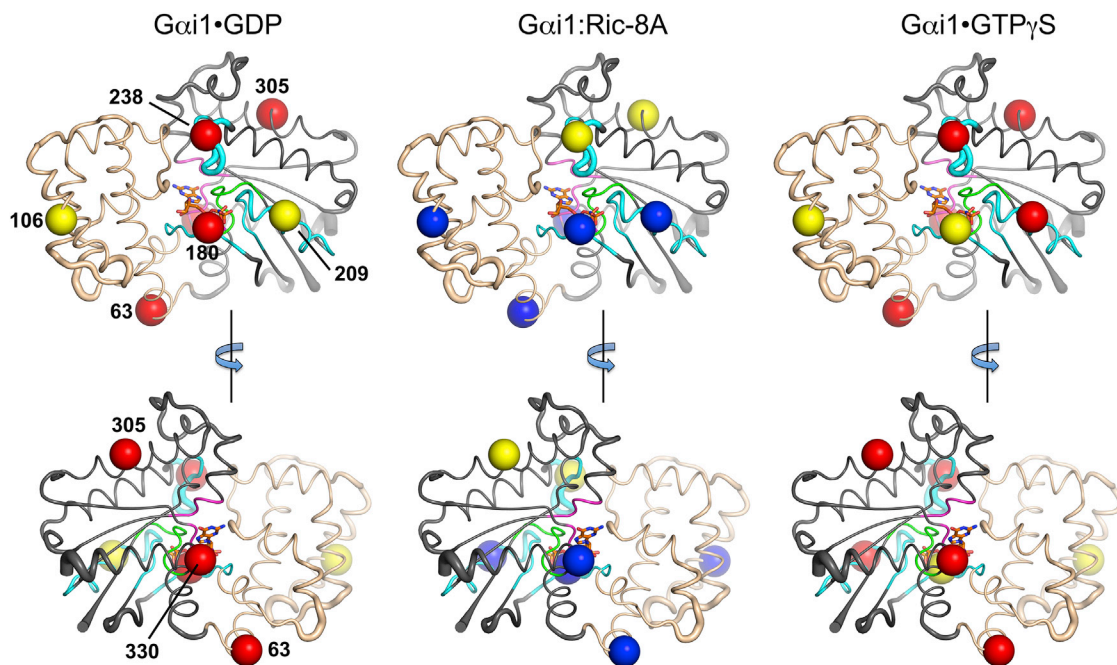


FIGURE 4 Heat maps constructed from  $\phi_{\text{local}}$  values listed in Table 2. Red,  $\phi < 1.5$  ns; yellow,  $\phi \geq 1.5$  ns and  $< 2$  ns; blue,  $\phi \geq 2$  ns.

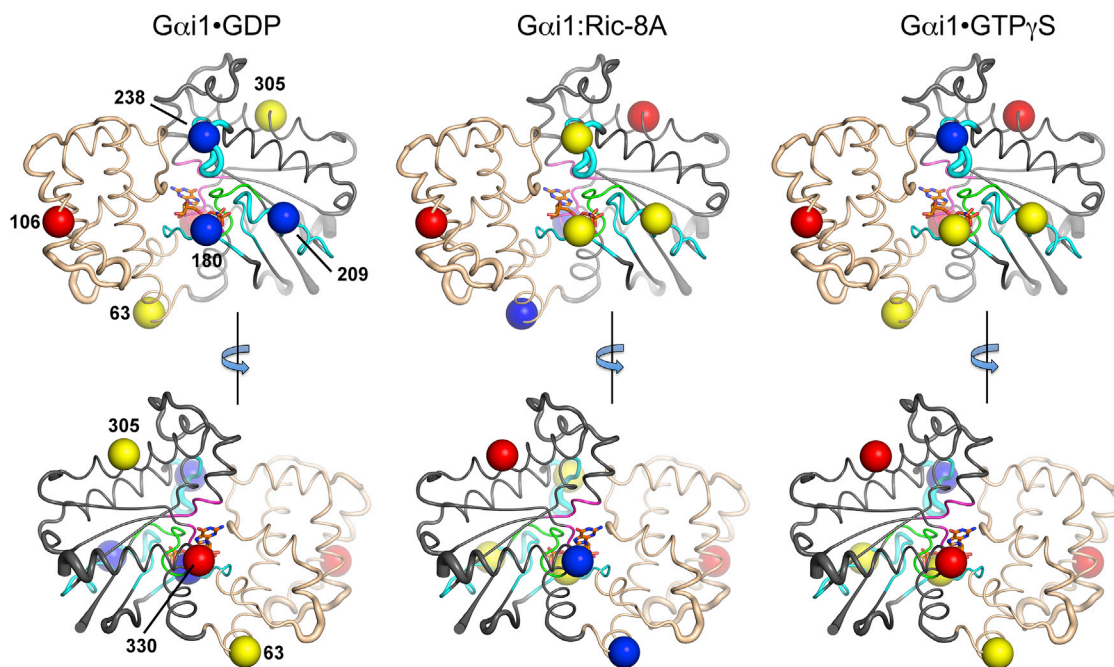


FIGURE 5 Heat maps constructed from  $S^2$  values listed in Table 2. Red,  $S^2 < 0.50$ ; yellow,  $S^2 > 0.50$  and  $\leq 0.70$ ; blue,  $S^2 > 0.70$ .

motions in timescales ranging from milliseconds to nanoseconds.

As a consequence of interactions with  $Mg^{2+}$  and the nucleotide  $\gamma$ -phosphate, Switch I and II both become well ordered in *Gai1* complexes with GTP analogs (12,48). The transition to a longer local correlation time at Ax180 is consistent with the emergence of an immobilized component in the EPR spectrum of a spin label at position 180 of *Gai1*•GTP $\gamma$ S, which may be in slow exchange with more highly mobile species (20,49). The transition of Ax209 to faster dynamics in *Gai1*•GTP $\gamma$ S is reflected in the EPR spectrum, which reveals a single state in fast anisotropic motion, consistent with rapid local motion of a solvent-exposed residue (46). In contrast, the relaxation-dispersion studies referenced above show that these and other regions of *Gai1* show dynamics at millisecond-to-microsecond timescales (47).

In both the GDP and GTP $\gamma$ S-bound states, the order parameters for Alexa fluorophores in the three switch segments are the highest of the labeled sites. The order parameters for Ax180 and Ax209 are lower in *Gai1*•GTP $\gamma$ S, which is a paradoxical finding considering the rigidification of Switch I and II observed in crystal structures. Decreases in order parameters, particularly at Ax180 ( $S^2$ , 0.88  $\rightarrow$  0.70) could result from a transition to longer-range backbone motion, or reflect increased anisotropic motion.

The local correlation times of Alexa fluorophores at sites beyond the switch regions are relatively unaffected by nucleotide exchange. This is expected from the

absence of structural changes, or relative changes, in crystallographic B factors at the interdomain hinge (Ax63), the HD (Ax106), the purine-binding site (Ax330), and  $\alpha$ 4 (Ax305) in the corresponding crystal structures of *Gai1*. The order parameters are likewise insensitive to substitution of GDP with GTP $\gamma$ S, with the exception of Ax305, for which motion appears to be significantly less restricted in the GTP $\gamma$ S state ( $S^2$ , 0.57  $\rightarrow$  0.28), which exhibits the highest sampling volume for local dynamics of any of the sites or *Gai1* species. This result is surprising because crystal structures of *Gai1* do not show the neighborhood of residue Ax305, a well-ordered  $\alpha$  helix, to be conformationally labile in any of several nucleotide- or effector/regulator-bound states. Other solution studies, however, have revealed dynamic processes in  $\alpha$ 4. A nitroxide spin label at position 300, a buried residue 1.5 turn of helix upstream of Ax305, is shown to be highly mobile in the *Gai1*:GTP $\gamma$ S complex (46). However, an immobilized population of conformational states appears in the GDP-bound species and is dominant in the GPCR (rhodopsin-bound) complex with *Gai1*-containing G protein heterotrimers, indicative of allosteric coupling between  $\alpha$ 4 and the nucleotide-,  $G\beta\gamma$ -, and GPCR-binding sites.

### Ric-8A induced changes in local dynamics

Alexa fluorophores at four sites in *Gai1* report two-fold increases in local correlation time in the complex with Ric-8A, relative to *Gai1*•GDP. Two are in Switch segments

I and II respectively, Ax180 ( $\phi_{local}$ , 1.3  $\rightarrow$  2.7 ns) and Ax209 ( $\phi_{local}$ , 1.6  $\rightarrow$  2.8 ns), another near the purine binding site, Ax330 ( $\phi_{local}$ , 1.1  $\rightarrow$  2.3 ns), and the fourth at the inter-domain hinge, Ax63 ( $\phi_{local}$ , 1.2  $\rightarrow$  2.3 ns). The slower dynamics at these sites may be indicative of an interconversion between conformational states or long-range coupling with neighboring structural elements, either of which could result from the involvement of nearby residues in direct contact with Ric-8A. EPR experiments demonstrated that nitroxide spin labels at residues 180 and 209 become partially immobilized upon Ric-8A binding (20). At the Switch II site, the immobilized component is dominant. The high uncertainty in  $\phi_{local}$  is suggestive of conformational heterogeneity or long-range coupling, as discussed above. Although Ax180 and Ax209 exhibit slower motion in the Ric-8A-bound state, they show only a slight reduction in order parameter relative to  $G\alpha\bullet$ GDP, which does not exceed the confidence limits. Ax238 in Switch III experiences a modest reduction in order parameter in the Ric-8A bound state, although there is no evidence for direct perturbation of this residue from EPR studies (20).

The increase in local correlation time at Ax330, near the purine-binding site  $\beta 6-\alpha 5$ , is likely a consequence of GDP release. Double electron-electron resonance spectra of  $G\alpha 1$ :Ric-8A show evidence of global plasticity in the spatial disposition at residue 330 with respect to residue 43 in the phosphate-binding loop and residue 305 in the  $\alpha 4$  helix. Ax330 is more highly ordered ( $S^2$ , 0.48  $\rightarrow$  0.73) in the Ric-8A-bound complex than in either nucleotide-bound state, which may reflect restricted anisotropic motion (32). Nitroxide spin-labeled 330 also exhibits spectra characteristic of strong immobilization in the complex of heterotrimeric Gi with Rhodopsin (41).

At the interdomain hinge in the  $G\alpha 1$ :Ric-8A complex, Ax63 reports increases in both local correlation time and, like Ax330, order ( $S^2$ , 0.56  $\rightarrow$  0.73) relative to  $G\alpha 1\bullet$ GDP, indicating an increase in local rigidity when Ric-8A is bound. In view of the observation that the HD and RD move apart more than 20 Å during GPCR and Ric-8A-catalyzed nucleotide exchange (15,20), it is likely that the secondary-structure dynamics involving the HD-RD interface are significantly altered. The time-resolved anisotropy data indicate that Ric-8A binding results in a significant reduction in the local dynamics at the domain hinge, and possibly long-range correlated motions. Ric-8A may contact  $G\alpha 1$  directly in this region.

At the remaining sites in the  $G\alpha 1$ :Ric-8A complex (Ax106, Ax238, and Ax305), we observe a 10–20% increase in  $\phi_{local}$  relative to either nucleotide-bound state, suggesting significant immobilization at these sites. The differences, however, are within the confidence limits of  $\phi_{local}$ . We do observe a significant increase in  $S^2$  for the interdomain hinge residue Ax63, which tracks with the larger increment in  $\phi_{local}$  described above. The order parameter for Ax305 in  $\alpha 4$  is similar to that observed for  $G\alpha 1\bullet$ GDP.

Notably, neither  $\phi_{local}$  nor  $S^2$  of the helical-domain reporter Ax106 is significantly different in the  $G\alpha 1\bullet$ GDP,  $G\alpha 1\bullet$ GTP $\gamma$ S, or nucleotide-free  $G\alpha 1$ :Ric-8A complexes.

## CONCLUSIONS

Here, we resolved the timescales of the dynamics of secondary-structure elements within  $G\alpha 1$  when bound to nucleotides or to the GEF/chaperone Ric-8A. The data indicate that the local dynamics of  $G\alpha 1$  is, for the most part, relatively insensitive to the exchange of GTP $\gamma$ S and Mg<sup>2+</sup> for GDP. The Alexa reporter at Switch II, which shows a significant increase in the rate of local dynamics, is an exception. This finding is consistent with recent NMR results (47), EPR experiments (15,20,41,46,49), and crystal structures (12,43,48), which together show that Switch II becomes more ordered and conformationally homogeneous in the GTP-bound state, which binds more tightly to  $G\alpha$  effectors but also undergoes faster nanosecond-scale dynamics.

The timescales of local dynamics at many sites in  $G\alpha 1$  are significantly perturbed upon binding of Ric-8A to  $G\alpha 1\bullet$ GDP, with subsequent release of GDP. The changes are consistent with evidence that Ric-8A binding induces a molten-globule-like state (19), in which regions within the RD become more flexible and adopt an ensemble of states that exchange slowly, as reflected in longer local correlation times (see, for example, reference (50)). When bound to Ric-8A,  $G\alpha 1$  exhibits large domain-domain displacements and intra-RD structural heterogeneity (20). The slow dynamics observed in  $G\alpha 1$  structural elements that are involved in nucleotide binding may be reflective of Ric-8A-induced perturbations that disrupt favorable van der Waals, hydrogen bond, and electrostatic interactions with GDP. The onset of such effects would provide a mechanism for release of the GDP nucleotide residing in the binding site between the two domains.

## SUPPORTING MATERIAL

Supporting Materials and Methods and six figures are available at [http://www.biophysj.org/biophysj/supplemental/S0006-3495\(16\)30587-2](http://www.biophysj.org/biophysj/supplemental/S0006-3495(16)30587-2).

## ACKNOWLEDGMENTS

We thank Heidi E. Hamm (Vanderbilt University) and Suzanne F. Scarlata (Worcester Polytechnic Institute) for providing HEXA I  $G\alpha 1$  template DNA and mutants, and Anita M. Preininger (Vanderbilt University) for advice on expression and purification. We thank Bruce Bowler, T.C. Mou, and Levi McClelland (University of Montana) for the use of instrumentation for purification and functional protein assays. We thank Baisen Zeng for providing Ric-8A.

This work was supported by National Institutes of Health (NIH) grant R01GM105993 (S.R.S.). Fluorescence measurements and analyses were performed in the BioSpectroscopy Core Research Laboratory at the University of Montana, which is operated with support from NIH Centers of Biomedical Research Excellence (CoBRE) Award P20GM103546 to the Center for Biomolecular Structure and Dynamics, and from the Vice

President of Research and Creative Scholarship at the University of Montana. The MALDI-TOF instrument at the University of Montana, which was used for protein characterization, was purchased with funds from the National Science Foundation (award CHE-1039814) and operated with support from NIH CoBRE Award P20GM103546 to the Center for Biomolecular Structure and Dynamics.

## SUPPORTING CITATIONS

References (51–55) appear in the Supporting Material.

## REFERENCES

- Gilman, A. G. 1987. G proteins: transducers of receptor-generated signals. *Annu. Rev. Biochem.* 56:615–649.
- Sprang, S. R. 1997. G protein mechanisms: insights from structural analysis. *Annu. Rev. Biochem.* 66:639–678.
- Tall, G. G., A. M. Krumins, and A. G. Gilman. 2003. Mammalian Ric-8A (synembryn) is a heterotrimeric G $\alpha$  protein guanine nucleotide exchange factor. *J. Biol. Chem.* 278:8356–8362.
- Chan, P., M. Gabay, ..., G. G. Tall. 2011. Ric-8B is a GTP-dependent G protein alphas guanine nucleotide exchange factor. *J. Biol. Chem.* 286:19932–19942.
- Hinrichs, M. V., M. Torrejón, ..., J. Olate. 2012. Ric-8: different cellular roles for a heterotrimeric G-protein GEF. *J. Cell. Biochem.* 113:2797–2805.
- Blumer, J. B., and S. M. Lanier. 2014. Activators of G protein signaling exhibit broad functionality and define a distinct core signaling triad. *Mol. Pharmacol.* 85:388–396.
- Tall, G. G. 2013. Ric-8 regulation of heterotrimeric G proteins. *J. Recept. Signal Transduct. Res.* 33:139–143.
- Papasergi, M. M., B. R. Patel, and G. G. Tall. 2015. The G protein  $\alpha$  chaperone Ric-8 as a potential therapeutic target. *Mol. Pharmacol.* 87:52–63.
- Lambright, D. G., J. P. Noel, ..., P. B. Sigler. 1994. Structural determinants for activation of the alpha-subunit of a heterotrimeric G protein. *Nature.* 369:621–628.
- Oldham, W. M., and H. E. Hamm. 2006. Structural basis of function in heterotrimeric G proteins. *Q. Rev. Biophys.* 39:117–166.
- Sprang, S. R., Z. Chen, and X. Du. 2007. Structural basis of effector regulation and signal termination in heterotrimeric G $\alpha$  proteins. *Adv. Protein Chem.* 74:1–65.
- Coleman, D. E., A. M. Berghuis, ..., S. R. Sprang. 1994. Structures of active conformations of G $\alpha$ 1 and the mechanism of GTP hydrolysis. *Science.* 265:1405–1412.
- Noel, J. P., H. E. Hamm, and P. B. Sigler. 1993. The 2.2 Å crystal structure of transducin- $\alpha$  complexed with GTP  $\gamma$ S. *Nature.* 366:654–663.
- Rosenbaum, D. M., S. G. Rasmussen, and B. K. Kobilka. 2009. The structure and function of G-protein-coupled receptors. *Nature.* 459:356–363.
- Van Eps, N., A. M. Preininger, ..., W. L. Hubbell. 2011. Interaction of a G protein with an activated receptor opens the interdomain interface in the alpha subunit. *Proc. Natl. Acad. Sci. USA.* 108:9420–9424.
- Rasmussen, S. G., B. T. DeVree, ..., B. K. Kobilka. 2011. Crystal structure of the  $\beta$ 2 adrenergic receptor-Gs protein complex. *Nature.* 477:549–555.
- Westfield, G. H., S. G. Rasmussen, ..., G. Skiniotis. 2011. Structural flexibility of the G $\alpha$ s alpha-helical domain in the beta2-adrenoceptor Gs complex. *Proc. Natl. Acad. Sci. USA.* 108:16086–16091.
- Dror, R. O., T. J. Mildorf, ..., D. E. Shaw. 2015. Signal transduction. Structural basis for nucleotide exchange in heterotrimeric G proteins. *Science.* 348:1361–1365.
- Thomas, C. J., K. Briknarová, ..., S. R. Sprang. 2011. The nucleotide exchange factor Ric-8A is a chaperone for the conformationally dynamic nucleotide-free state of G $\alpha$ 1. *PLoS One.* 6:e23197.
- Van Eps, N., C. J. Thomas, ..., S. R. Sprang. 2015. The guanine nucleotide exchange factor Ric-8A induces domain separation and Ras domain plasticity in G $\alpha$ 1. *Proc. Natl. Acad. Sci. USA.* 112:1404–1409.
- Medkova, M., A. M. Preininger, ..., H. E. Hamm. 2002. Conformational changes in the amino-terminal helix of the G protein alpha(i1) following dissociation from Gbetagamma subunit and activation. *Biochemistry.* 41:9962–9972.
- Minazzo, A. S., R. C. Darlington, and J. B. A. Ross. 2009. Loop dynamics of the extracellular domain of human tissue factor and activation of factor VIIa. *Biophys. J.* 96:681–692.
- Nitsche, J. M., H. C. Chang, ..., B. J. Nicholson. 2004. A transient diffusion model yields unitary gap junctional permeabilities from images of cell-to-cell fluorescent dye transfer between *Xenopus* oocytes. *Biophys. J.* 86:2058–2077.
- Petrásek, Z., and P. Schwille. 2008. Precise measurement of diffusion coefficients using scanning fluorescence correlation spectroscopy. *Biophys. J.* 94:1437–1448.
- Kapusta, P. 2010. Absolute Diffusion Coefficients: Compilation of Reference Data for FCS Calibration. PicoQuant, Berlin.
- Belford, G. G., R. L. Belford, and G. Weber. 1972. Dynamics of fluorescence polarization in macromolecules. *Proc. Natl. Acad. Sci. USA.* 69:1392–1393.
- Small, E. W., and I. Isenberg. 1977. Hydrodynamic properties of a rigid molecule: rotational and linear diffusion and fluorescence anisotropy. *Biopolymers.* 16:1907–1928.
- Lakowicz, J. R. 2006. Principles of Fluorescence Spectroscopy, 3rd ed. Springer Science, New York.
- Li, Z., S. Raychaudhuri, and A. J. Wand. 1996. Insights into the local residual entropy of proteins provided by NMR relaxation. *Protein Sci.* 5:2647–2650.
- Scott, D. R., C. F. Vardeman, 2nd, ..., B. M. Baker. 2012. Limitations of time-resolved fluorescence suggested by molecular simulations: assessing the dynamics of T cell receptor binding loops. *Biophys. J.* 103:2532–2540.
- Rusinova, E., V. Tretyachenko-Ladokhina, ..., J. B. Alexander Ross. 2002. Alexa and Oregon Green dyes as fluorescence anisotropy probes for measuring protein-protein and protein-nucleic acid interactions. *Anal. Biochem.* 308:18–25.
- Gu, Y., D. W. Li, and R. Brüschweiler. 2015. Decoding the mobility and time scales of protein loops. *J. Chem. Theory Comput.* 11:1308–1314.
- Scouras, A. D., and V. Daggett. 2011. The Dynameomics rotamer library: amino acid side chain conformations and dynamics from comprehensive molecular dynamics simulations in water. *Protein Sci.* 20:341–352.
- Ries, J., and P. Schwille. 2012. Fluorescence correlation spectroscopy. *BioEssays.* 34:361–368.
- Kinosita, K., Jr., A. Ikegami, and S. Kawato. 1982. On the wobbling-in-cone analysis of fluorescence anisotropy decay. *Biophys. J.* 37:461–464.
- Jähnig, F. 1979. Structural order of lipids and proteins in membranes: evaluation of fluorescence anisotropy data. *Proc. Natl. Acad. Sci. USA.* 76:6361–6365.
- Bayley, P., S. Martin, ..., C. Royer. 2003. Time-resolved fluorescence anisotropy studies show domain-specific interactions of calmodulin with IQ target sequences of myosin V. *Eur. Biophys. J.* 32:122–127.
- Kim, T. Y., T. Schlieter, ..., U. Alexiev. 2012. Activation and molecular recognition of the GPCR rhodopsin—insights from time-resolved fluorescence depolarisation and single molecule experiments. *Eur. J. Cell Biol.* 91:300–310.
- Alexiev, U., I. Rimke, and T. Pöhlmann. 2003. Elucidation of the nature of the conformational changes of the EF-interhelical loop in bacteriorhodopsin and of the helix VIII on the cytoplasmic surface of bovine rhodopsin: a time-resolved fluorescence depolarization study. *J. Mol. Biol.* 328:705–719.

40. Schröder, G. F., U. Alexiev, and H. Grubmüller. 2005. Simulation of fluorescence anisotropy experiments: probing protein dynamics. *Biophys. J.* 89:3757–3770.
41. Oldham, W. M., N. Van Eps, ..., H. E. Hamm. 2006. Mechanism of the receptor-catalyzed activation of heterotrimeric G proteins. *Nat. Struct. Mol. Biol.* 13:772–777.
42. Scheerer, P., J. H. Park, ..., O. P. Ernst. 2008. Crystal structure of opsin in its G-protein-interacting conformation. *Nature.* 455:497–502.
43. Mixon, M. B., E. Lee, ..., S. R. Sprang. 1995. Tertiary and quaternary structural changes in Gi alpha 1 induced by GTP hydrolysis. *Science.* 270:954–960.
44. Berghuis, A. M., E. Lee, ..., S. R. Sprang. 1996. Structure of the GDP-Pi complex of Gly203→Ala g $\alpha$ 1: a mimic of the ternary product complex of g $\alpha$ -catalyzed GTP hydrolysis. *Structure.* 4:1277–1290.
45. Coleman, D. E., and S. R. Sprang. 1998. Crystal structures of the G protein Gi alpha 1 complexed with GDP and Mg<sup>2+</sup>: a crystallographic titration experiment. *Biochemistry.* 37:14376–14385.
46. Van Eps, N., W. M. Oldham, ..., W. L. Hubbell. 2006. Structural and dynamical changes in an alpha-subunit of a heterotrimeric G protein along the activation pathway. *Proc. Natl. Acad. Sci. USA.* 103:16194–16199.
47. Goricanec, D., R. Stehle, ..., F. Hagn. 2016. Conformational dynamics of a G-protein alpha subunit is tightly regulated by nucleotide binding. *Proc. Natl. Acad. Sci. USA.* 113:E3629–E3638.
48. Coleman, D. E., and S. R. Sprang. 1999. Structure of G $\alpha$ 1.GppNHp, autoinhibition in a g $\alpha$  protein-substrate complex. *J. Biol. Chem.* 274:16669–16672.
49. Oldham, W. M., N. Van Eps, ..., H. E. Hamm. 2007. Mapping allosteric connections from the receptor to the nucleotide-binding pocket of heterotrimeric G proteins. *Proc. Natl. Acad. Sci. USA.* 104:7927–7932.
50. Chakraborty, S., V. Ittah, ..., Z. Peng. 2001. Structure and dynamics of the alpha-lactalbumin molten globule: fluorescence studies using proteins containing a single tryptophan residue. *Biochemistry.* 40:7228–7238.
51. Medina, M. A., and P. Schwille. 2002. Fluorescence correlation spectroscopy for the detection and study of single molecules in biology. *BioEssays.* 24:758–764.
52. Bacia, K., and P. Schwille. 2007. Fluorescence correlation spectroscopy. *Methods Mol. Biol.* 398:73–84.
53. Bacia, K., E. Haustein, and P. Schwille. 2014. Fluorescence correlation spectroscopy: principles and applications. *Cold Spring Harb. Protoc.* 2014:709–725.
54. Bohmer, M., M. Wahl, ..., J. Enderlein. 2002. Time-resolved fluorescence correlation spectroscopy. *Chem. Phys. Lett.* 353:439–445.
55. Enderlein, J., and I. Gregor. 2005. Using fluorescence lifetime for discriminating detector afterpulsing in fluorescence-correlation spectroscopy. *Rev. Sci. Instrum.* 76:033102.
56. Straume, M., S. G. Frasier-Cadoret, and M. L. Johnson. 1991. Least-squares analysis of fluorescence data. In *Topics in Fluorescence Spectroscopy, Vol. 2*. J. R. Lakowicz, editor. Kluwer Academic Publishers, Dordrecht, The Netherlands.